Applied Physics A (2022) 128:89
https://doi.org/10.1007/s00339-021-05228-8

Applied Physics A
Materials Science & Processing

Copper phthalocyanine-borophene nanocomposite-based non-enzymatic electrochemical urea biosensor

Saliha Güngör[1] · Cihat Taşaltın[2] · İlke Gürol[2] · Gülsen Baytemir[1] · Selcan Karakuş[3] · Nevin Taşaltın[1,4]

Received: 3 December 2021 / Accepted: 21 December 2021 / Published online: 5 January 2022

Abstract

Highly sensitive detection of urea is important and necessary in a wide variety of areas such as clinical diagnostics, environmental monitoring, and food safety applications. Herein, we demonstrated the fabrication of the sonochemical synthesized copper phthalocyanine (CuPc)-borophene nanocomposites-based non-enzymatic electrochemical biosensor for the urea detection at room temperature. The prepared CuPc, borophene, and CuPc-borophene nanocomposite were characterized using different techniques such as scanning electron microscopy, high-resolution transmission electron microscopy, X-ray diffraction, Fourier transform infrared spectroscopy, and Raman spectroscopy. With the surface and chemical advantages of CuPc-borophene nanocomposite, urea detection performances of the CuPc-borophene nanocomposite-based biosensors exhibited a high selectivity in many matrices such as glucose, fructose, lactose, and maltose, even in highly complex isotonic solutions containing competitive ions at room temperature. CuPc-borophene nanocomposite-based sensor exhibited higher sensitivity of 10.43 μA/mMcm^2 against (250–1000) μM with a detection limit of 0.05 μM in voltammetric cycle of 60 s due to high charge transport advantages of borophene additive. Experimental results revealed that the CuPc-borophene nanocomposite-based non-enzymatic electrochemical biosensor was a sensitive, stable, rapid, portable, and low-cost. Furthermore, the biosensor is a promising candidate for urea electrochemical analysis in a complex aqueous medium for biomedical applications.

Keywords Copper phthalocyanine · Dye · Borophene · Nanocomposite · Sensor · Urea

1 Introduction

A high level of urea in the blood is a sign of kidney failure, stomach, and intestinal disorders, while low urea levels are a sign of liver failure. The normal urea concentration level in body fluids such as urine and blood serum is between 2.7 and 7.5 mM [1–3]. Therefore, rapid and accurate determination of urea in blood is highly demanded clinically. Electrochemical, colorimetric, fluorescence, chemiluminescence, and surface plasmon resonance methods are available for urea detection. The most remarkable method is the non-enzymatic electrochemical method [4–9] due to its easy use, short response time, high sensitivity, continuous monitoring, and low-cost advantages.

Phthalocyanines (Pcs) are aromatic macrocyclic dyes with high electronic displacement, intense absorption, high thermal and photochemical stability, and electrocatalytic properties [10–15]. These properties of phthalocyanines ensure high performance of Pc-based gas sensors and biosensors [16–20]. Metallophthalocyanines (MPcs) possess an N4-coordination site for metal ions (e.g., Cu, Ni, Co, Zn, Fe, Ti, V, and Mn) and extended π-systems, endowing them with excellent redox activity and catalytic property [16]. CuPcs dyes are used in many fields such as chemical sensors [17], semiconductors [18], photoconductors [21], electrochromic displays [19], electro-optical materials [20] due to their properties high electrocatalytic effect. Only a

✉ Selcan Karakuş
selcan@iuc.edu.tr

✉ Nevin Taşaltın
nevintasaltin@maltepe.edu.tr

[1] Department of Electrical and Electronics Engineering, Maltepe University, 34857 Istanbul, Turkey

[2] Materials Institute, TUBITAK Marmara Research Center, 41470 Kocaeli, Turkey

[3] Department of Chemistry, Faculty of Engineering, Istanbul University-Cerrahpasa, 34320 Istanbul, Turkey

[4] Basic Sciences, Maltepe University, 34857 Istanbul, Turkey

few phthalocyanines from the phthalocyanine family have been used in biosensor applications. CoPc has been used as redox mediators in enzymatic glucose biosensors [22]. It has been reported that zinc phthalocyanine (ZnPc) is not stable in the biosensor due to its weak electrochemical activity and low electrical conductivity [23]. Therefore, graphene nanosheets and carbon nanotubes (CNTs) have been used as additives in metallophthalocyanines (MPc) to increase the electron transfer and electrical conductivity of MPc [24–27]. Furthermore, it has been reported that when MPc and graphene oxide (GO) are composited, there is a strong π-π interaction between MPc and GO and thus the biosensor exhibits a stable response. Since 2015, theoretical and experimental research has been carried out on borophene nanosheet, which is two-dimensional boron nanostructure. A monolayer preparation of borophene by chemical vapor deposition (CVD) has been investigated [28–32]. The preparation of a few-layered borophene by the wet-chemistry started in 2018 [33–36]. The unique physical, chemical, and electronic properties of borophene have been reported in theoretical and experimental reports [28–36]. These properties suggest a wide range of applications of borophene-based materials such as polymer-borophene nanocomposites and Pc-borophene nanocomposites for electrochemical energy storage devices such as sensors, catalysts, batteries, and supercapacitors. The sonochemical method is extremely useful for the preparation of functional nanostructured materials and is frequently applied. This method enables the preparation of functional nanostructured materials with great homogeneity and the process to be more controlled compared to other nanocomposite preparation methods [37].

In enzymatic electrochemical urea sensors, in general, the urea detection mechanism can be explained based on two reactions: (a) Catalytic reaction and (b) Oxidation/reduction of sensing material [38–41]. The catalytic reaction of urea releases three ions from uncharged urea, 2 NH^+, and CO^- (Eqs. 1.1 and 1.2). These ions enable to increase the conductivity of the sensing material by providing more electrons to the conduction band of the sensing material. In addition, atmospheric oxygen molecules adsorb on surface of the sensing material and become ionized by removing an electron from the conduction band as they move from one region to the other on the surface and thus ionize as O_{ads}^- at the surface.

$$NH_2CONH_2 + 2H_2ONH_4^+ + CO_3^{2-} \quad (1.1)$$

$$R + O_{ads}^- \rightarrow RO + e^- \quad (1.2)$$

There is only one report on the Pc-based non-enzymatic electrochemical urea biosensor at room temperature [42]. The biosensor is zinc phthalocyanine/graphene oxide (ZnPc/GO) nanocomposite-based enzymatic amperometric electrochemical urea biosensor at room temperature. The biosensor detected urea in the range of (0.4–22 µM) with a detection limit of 0.034 µM. The existence of the points that need to be researched, the process steps, and the need to reduce the cost have been the driving force and the motivation in this research focusing on the preparation of novel non-enzymatic biosensor for urea detection at room temperature. In this regard, in this study, urea detection performances of the CuPc and CuPc-borophene nanocomposite-based non-enzymatic voltammetric electrochemical biosensors were investigated at room temperature in detail.

2 Experimental

The copper(II) phthalocyanine (CuPc) is a metallophthalocyanine that is copper(2 +) forming a coordination complex with phthalocyanine. CuPc was synthesized using the method which was reported in our previous study [43]. Furthermore, borophene nanosheets were prepared using a green ultrasonic irradiation method which was described in our previous study [44]. 1 mg of CuPc dissolved in 3 ml of chloroform and stirred for 5 min at room temperature to obtain the CuPc solution. 1 mg of borophene was added to the CuPc solution, rapidly stirred, and sonicated at 50 W for 15 min at room temperature under a nitrogen atmosphere to prevent from contamination.

CuPc and CuPc-borophene nanocomposite were coated on gold electrochemical transducers using a drop-casting method, and the prepared films were dried at 40 °C to obtain CuPc and CuPc-borophene nanocomposite-based non-enzymatic electrochemical sensors. In the analyte preparation process, urea analytes with a urea concentration range of (250–1000) µM were prepared in phosphate buffer solution (PBS) for urea detection measurements. The prepared biosensors were tested using a 3-electrode cyclic voltammetry method (Ebtro Voltammetric Electrochemical Workstation) was used for all electrochemical tests. This method was based on the measurement of the current response based on the redox processes (reduction or oxidation reaction) in a solution to determine the selectivity and sensitivity of the prepared sensors. Tests of biosensors were carried out by placing each sensor in the electrochemical workstation, dropping each analyte sequentially starting from low concentration analyte on the sensing coatings and applying different scanning speeds in the range of $[-0.6, +0.6]$ V after each analyte drop, and recording the I–V characteristics of the sensor material. Before each test, the sensors were washed with distilled water. However, treatment with solvents such as chloroform and acetone, which can dissolve Pc, is avoided.

3 Results and discussion

The chemical and morphological properties of the CuPc, borophene, and the novel CuPc-borophene nanocomposite were determined using different techniques such as scanning electron microscopy (SEM) (SEM, FEI FEG QUANTA 450, gold coating and at the cooling temperature to 2 °C in vacuum), high-resolution transmission electron microscopy (HRTEM) (JEOL JEM-ARM200CFEG UHR-TEM), X-ray diffraction (XRD) (Rigaku Miniflex 600) (Cukα ($\lambda = 1.5406$ Å), Fourier transform infrared spectroscopy (FTIR) (Perkin Elmer, Spectrum Two, at a resolution of 4 cm^{-1}), and Raman spectroscopy (Renishaw in via Raman microscope, 2018 model). The HRTEM and XRD analysis results of the prepared borophene were given in Fig. 1. HRTEM results revealed that there were freestanding borophene nanosheets in DMF medium (Fig. 1a).

The morphology of the CuPc-borophene nanocomposite was monitored by the SEM technique. With this approach, the SEM micrograph of the CuPc-borophene nanocomposite was presented in Fig. 1d, e. SEM results showed that the CuPc-borophene nanocomposite had an irregular-shaped structure and was uniformly distributed all over the structure with the size of the particles within a size range of 300–500 nm. Figure 1d revealed that the prepared CuPc-borophene nanocomposite could be dispersed on the surface of polymer matrix via the assistance of a sonochemical exfoliation process, resulting to homogeneous dispersion of borophene on the CuPc matrix [45]. Furthermore, the EDX spectrum of CuPc-borophene nanocomposite was given in Fig. 1e. From the observation of corresponding elements mappings (SEM–EDX), it was observed that the prepared nanocomposite was only composed of B, Pt, C, N, O, F, and Cu elements and the result was similar to previous studies [46]. As it is known, β-rhombohedral boron is a complex structure with rhombohedral unit cell containing twenty types of B atom sites and the structure of the boron crystal is based on the B12 icosahedron shell motif. The regular icosahedron boron-rich solid is one of the classical regular polyhedrons in the convex polyhedrons of Euclidean space (regular tetrahedron, regular hexahedron (cube), regular octahedron, regular dodecahedron, and regular icosahedron) with five, three, and two axes of symmetry in the structure [47]. In this study, we used a green and low-cost sonochemical method to observe the physical exfoliation of layer borophenes under high-intensity ultrasonic waves, leading to the formation of microcavities in the liquid. Ultrasonic cavitations cause the process of growth and collapse of bubbles under the ultrasound. The collapse of these acoustic cavities produces the inter-sheet forces between layers of a bulk material, exfoliating the 2D nanomaterials by overcoming the interlayer van der Waals forces. Afterward, the centrifugation method is used to remove unexfoliated residues [48]. According to XRD result, we noticed that there was no phase change in the physical exfoliation process from boron microparticles to borophene and boron microparticles and borophene exhibited the β-rhombohedral phase and the same crystallinity. The prepared borophene nanosheets had a crystalline structure with lattice spacing of 0.41 nm. An individual borophene nanosheet was examined via the fast Fourier transform (FFT) diffraction pattern as shown in the inset of Fig. 2b. Furthermore, the crystallinity and phase of the borophene nanosheets were determined from the analysis of XRD (Fig. 2c). XRD peaks were corresponded to the (0001) plane of β-rhombohedra boron according to PDF31-0207 (the unit cell parameters: $a = 10.925$ Å, $b = 10.925$ Å, and $c = 23.814$ Å). Furthermore, the crystal system of the prepared β borophene was R-3 m (166). Characterization results were proved the formation of β phase of borophene and XRD patterns of the prepared borophene were indexed to the centrosymmetric β-rhombohedral borophene crystal structure [35, 49]. These experimental results were in good agreement with the HRTEM analysis of the prepared borophene. The HRTEM and XRD analysis results of the prepared borophene were given in Fig. 1. HRTEM results revealed that there were freestanding borophene nanosheets in DMF medium (Fig. 1a). The TEM image of the prepared borophene showed the formation of atomic sheets of borophene using the sonication method in the structure and verified the existence of β-rhombohedral phase of borophene. It was observed that the grain size of the sample was less than 10 nm. According to XRD result, we calculated the crystallite size of the borophene using the Scherrer equation (Eq. 2.1) [50].

$$D_p = \frac{0.94.\lambda}{\beta.\cos\theta} \tag{2.1}$$

where λ is the X-ray wavelength (0.15406), β is full width at half maximum (FWHM), and D is crystallite size diameter, and θ is Bragg's diffraction angle obtained from 2θ corresponding to maximum intensity of the XRD peak. The average crystallite size of the borophene was calculated from Scherer's equation. The average crystalline size of the prepared borophene was about 16.84 nm. These experimental results were in good agreement with the HRTEM analysis of the prepared borophene.

The borophene and CuPc-borophene nanocomposite were determined using FTIR technique to identify chemical bonds and functional groups of all samples and results were given in Fig. 2a, b. According to the FTIR peaks, it was observed that the characteristic peaks of

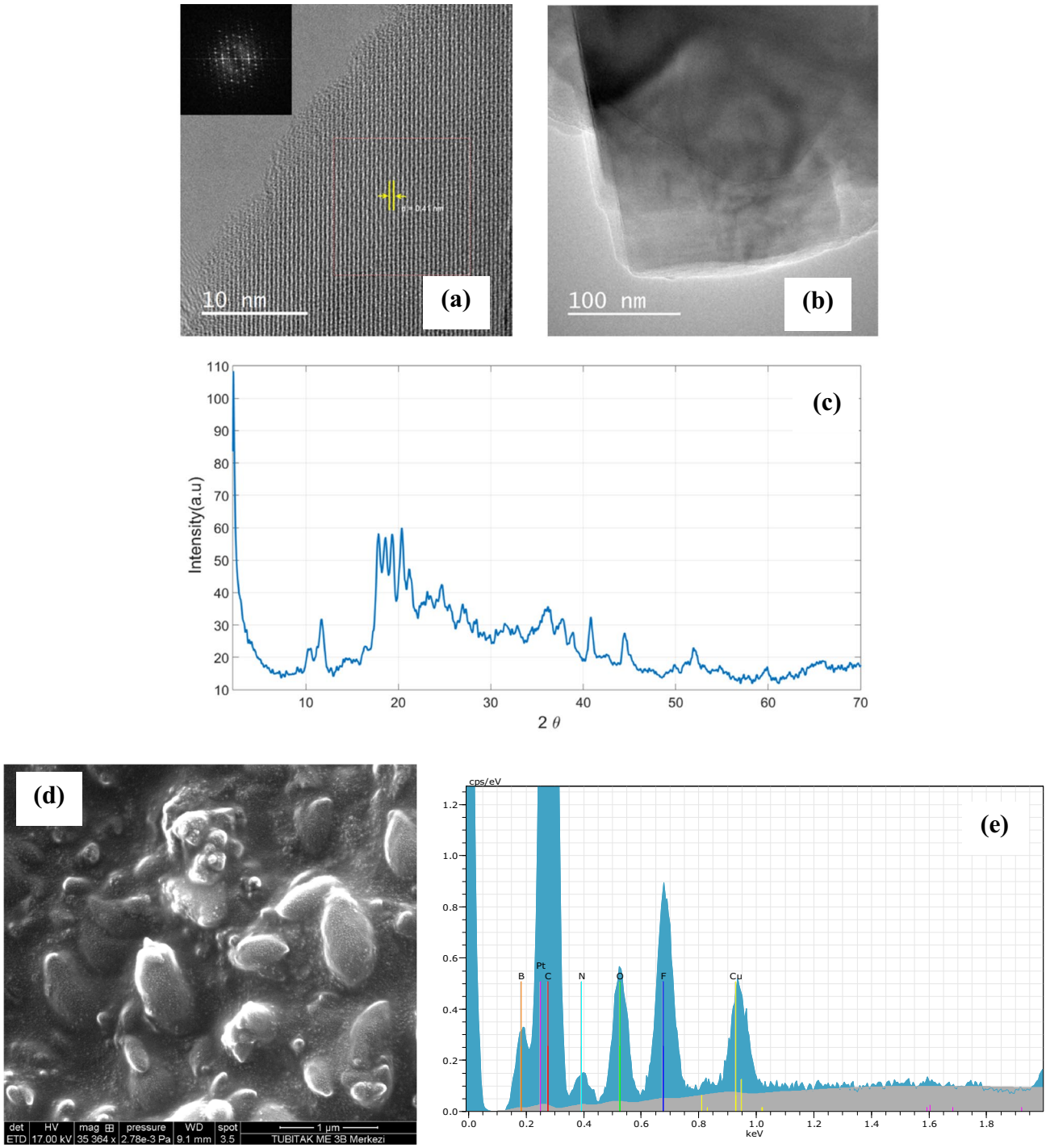

Fig. 1 **a** HRTEM image of the freestanding borophene nanosheets, **b** the borophene nanosheet with FFT diffraction, **c** XRD pattern of the borophene nanosheets, **d** SEM and **e** EDX images of CuPc-borophene nanocomposite

β_{12} borophene were observed at 3585 cm^{-1}, 2968 cm^{-1}, 2938 cm^{-1}, 1424 cm^{-1}, 1263 cm^{-1}, 1015 cm^{-1}, and 541 cm^{-1}, which were attributed to –OH, B–B, B–H, B–O, B–O–B vibrations, and sp^2 bonded h-BN, respectively [51, 52]. The characteristic peaks of the prepared CuPc-borophene nanocomposite were observed at 1591 cm^{-1} (C=N), 1491 cm^{-1} (C–C ring stretching), 1338 cm^{-1} (C=C of the benzene rings), 1284 cm^{-1} (C=N–C at bridge sites), 1199 cm^{-1} (Cu–N), and 799 cm^{-1} (C–H non-planar vibrations (out-of-plane bending). Furthermore, it was observed noted that the prepared CuPc-borophene nanocomposite was continuously utilizing the B–O, the stretching

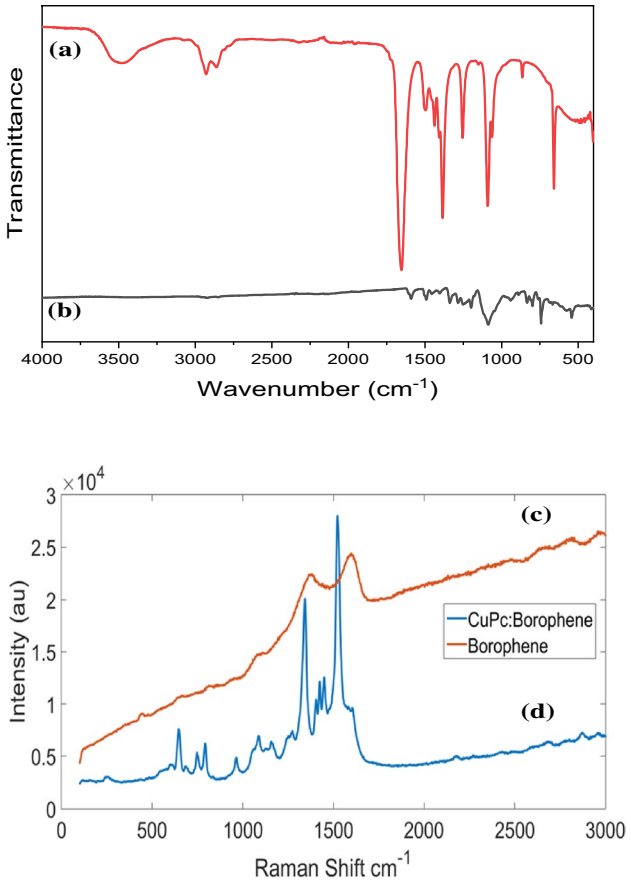

Fig. 2 FTIR results of **a** borophene and **b** CuPc-borophene nanocomposite, Raman spectroscopy analysis results of (c) borophene and (d) CuPc-borophene nanocomposite

vibration of boron-rich (or carbon-rich) B-C bonds, B–CR, and the B–O–B stretching characteristic peaks appeared at around 1455, 1250, 1087, and 742 cm^{-1} [53–56]. Two peaks at 2968 cm^{-1} and 2938 cm^{-1} in the borophene were detected while these peaks weren't observed in the CuPc-borophene nanocomposite. Additionally, a broad peak of -OH stretching at about 3510 cm^{-1}–3780 cm^{-1} was disappeared. Consequently, we concluded that the disappearance of the characteristic peaks of borophene and the appearance of characteristic peaks of the polymer matrix indicated that borophene was successfully encapsulated in the polymer matrix. FTIR results were found to be compatible with SEM results. The Raman spectroscopy analysis results of borophene and CuPc-borophene nanocomposite were given in Fig. 2c, d. The bands at 1129–1402 cm^{-1} in Raman spectrum of CuPc could be attributed to bending vibrations in isoindole and pyrrole moieties, while the bands at 1613–1425 cm^{-1} of CuPc were observed as benzene deformation according to the publications described before [44, 45]. In addition, the dependence of its wavelength on the Nα–M–Nα distance in CuPc was observed at 241, 264, 551, 586, 617, 648, 747, and 794 cm^{-1} in the Raman spectrum. The bands between 1400 and 1600 cm^{-1} in Raman spectrum of borophene could be attributed to inter-icosahedron bonds according to the previous publication [57–59]. The Raman bands of the borophene could be observed in the Raman spectrum of the CuPc-borophene nanocomposite. FTIR and Raman spectroscopies were used as fingerprint spectroscopic techniques due to the unique spectra of the prepared borophene nanosheets. The Raman and FTIR spectroscopies were complementary techniques and results were related to vibrational modes of characteristic functional groups in the prepared borophene nanosheets. In this study, we analyzed and discussed the structural parameters obtained by FTIR and Raman together. Using the FTIR spectra and Raman structural parameters, we observed the relationship between the functional groups of the prepared borophene and the formation of borophene with inter-icosahedron bonds.

Prepared biosensors were tested against urea in the range of (250–1000) µM. The measurements started with 0.125 mM urea concentration, and the urea was added continually to 1 mM. The sensitivity, the response time, and the limit of detection of the biosensors were determined in case of redox peaks in *I–V* characteristic with the occurrence of a redox reaction between the prepared CuPc-urea and CuPc-borophene nanocomposite-urea (Fig. 3). The electrocatalytic oxidation of urea was carried out through experiments by varying the sweep rate of cyclic voltammetry, allowing to be evaluating the electrochemical characteristics of the sensor-based CuPc-borophene nanocomposite. Based on the results described in Fig. 3, it can be possible to propose a mechanism for the biomimetic sensor. Initially the chemical step between the urea and the molecule of reduced CuPc promote the oxidation of urea and reduction of copper in the phthalocyanine in Fig. 3a. In the electrochemical step coupled to this chemical oxidation at the electrode surface, the re-oxidation of the metal (Cu^{+} to Cu^{2+}) in the CuPc leads to obtaining the anodic current observed due to the presence of urea in the measurement cell. However, the sensor response was increased when the sensor surface was modified with CuPc-borophene nanocomposite. Borophene nanocomposite could have enhanced to electrical conductivity properties of the CuPc (Fig. 3b). The sensitivities of the CuPc-based sensor and CuPc-borophene nanocomposite-based sensor are shown in Fig. 3c. The graph depicts that the CuPc-based sensor has a good sensitivity of 6.09 µA/mMcm^2, and CuPc-borophene nanocomposite has higher sensitivity of 10.43 µA/mMcm^2 in voltammetric cycle of 1 min with a detection limit of 0.05 µM. In CV-type sensor measurements, the recovery time is related to the total measurement time of the CV. Therefore, a clear recovery time cannot be mentioned. Recovery time and detection mechanism can be associated with CV-type sensors. Therefore, the speed of the

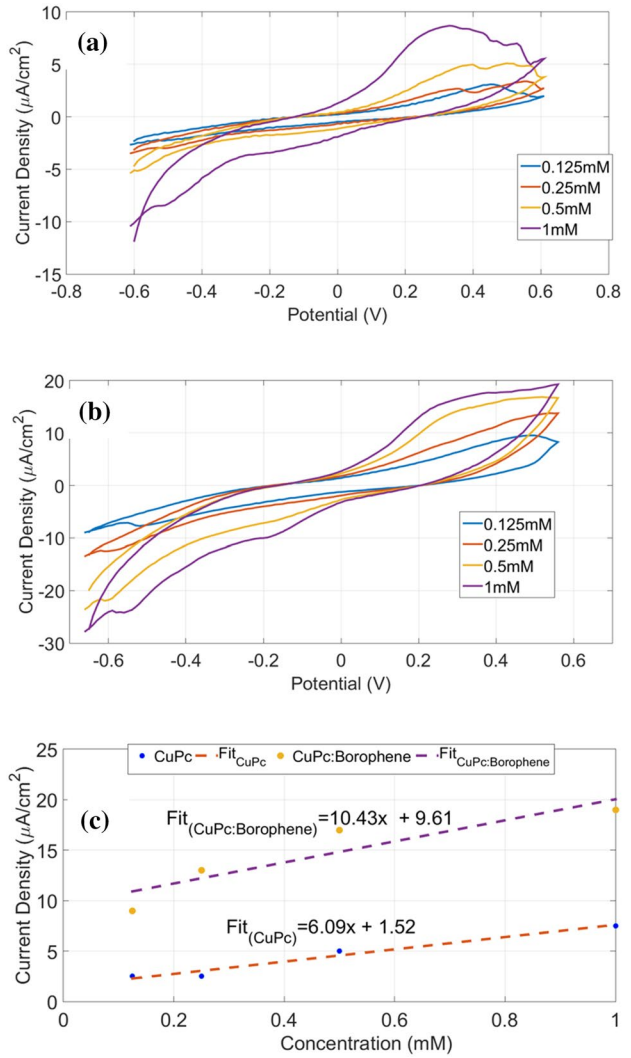

Fig. 3 Sensor responses of **a** CuPc against urea, **b** CuPc-borophene nanocomposite against urea, **c** Comparative sensitivities of CuPc and CuPc-borophene nanocomposite against urea

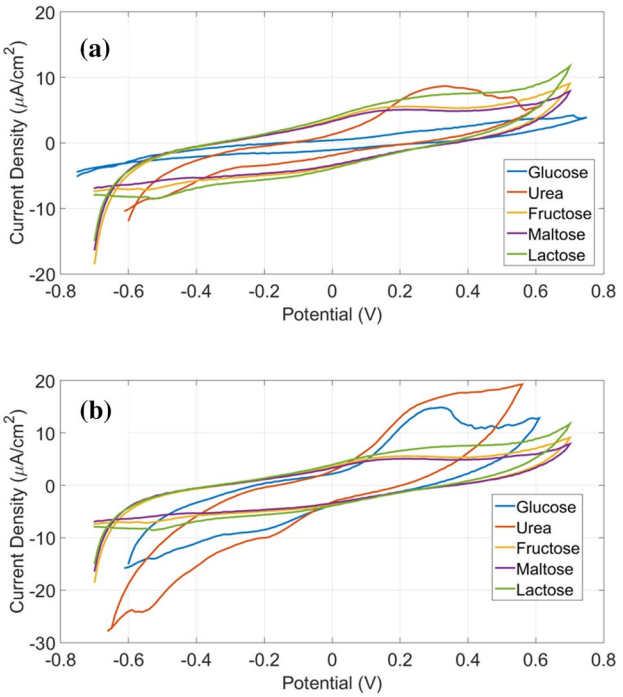

Fig. 4 Selectivity of **a** CuPc-based sensor, and **b** CuPc-borophene nanocomposite-based sensor

mechanism is the most important factor that determines the response and recovery time. In this study, 1 cycle of CV is completed in approximately 1 min.

Pc and borophene, which were used as sensing materials in the sensor, can work as electrochemical sensors. They do not undergo a structural change during the sensor application and the electrochemical interaction is a reversible process. This can be seen in the CV graphs in Fig. 3. At the end of the sensor measurements, it is not possible to find an analyte that has chemically bonded on the sensor materials. Furthermore, the selectivity tests of the sensors were carried out against 1 mM glucose, fructose, lactose, and maltose, respectively, Fig. 4a, b. The results reveal that the sensors are remarkably selective to urea. Moreover, the four individual sensors were prepared at similar conditions and tested against urea with same concentrations to investigate the repeatability of the sensor. The sensor results showed that the repeatability of the biosensor is acceptable. The stability of the biosensor was investigated after 2 months, and the peak currents for urea did not change, the sensors have good stability.

These results of the proposed biosensor were appreciable from the comparison with results of previous studies in the literature (Table 1). Comparison with the previous studies on Pc-based urea biosensor, there is only one report on the Pc-based non-enzymatic electrochemical urea biosensor at room temperature [60]. The biosensor is ZnPc/GO nanocomposite-based enzymatic amperometric electrochemical urea biosensor at room temperature. The biosensor detected urea in the range of (0.4–22 μM) with a detection limit of 0.034 μM. Among this, the prepared CuPc-borophene nanocomposite-based non-enzymatic voltammetric electrochemical urea biosensor has remarkable advantages such as easy handling process, low-cost without the cost of immobilization process, high sensitivity, high stability, and short response time. Although the stability of the sensor is good, physical deformation of the surface of the sensor or contamination on the surface is likely with many repeated measurements. For this reason, it cannot be predicted exactly how long-term multi-repeat use will produce results.

Cu^{2+} ion is known as one of the materials which can be effectively involved in redox reaction for the detection of urea by the non-enzymatic electrochemical approach [65]. In this study, we assumed that the proposed biosensor for the

Table 1 The comparison of analytical performance of the various electrodes for the detection of urea

Sample	Method	Range	LOD	Refs.
Ag NPs	Smartphone-assisted method	0.58–500 mM	0.0036 mM	[60]
Potentiometric urea biosensor	Enzymatic	0.01–500 mM	0.77 µM	[61]
Mercaptopropionic acid capped cadmium selenide quantum dots	Electrochemical	1–120 mM	1 mM	[62]
poly(diphenylamine)/phosphotungstic acid/graphene nanohybrid	Electrochemical	1–13 µM	–	[63]
Array-based titanium dioxide biosensor	Rtiometric	0.01 and 10 mM	2.4–5.5 µM	[64]
Zinc phthalocyanine/graphene oxide	Electrochemical	0.4–22 µM	0.034 µM	[42]
CuPc-borophene nanocomposite	Electrochemical	250–1000 µM	0.05 µM	This study

selective and sensitive sensing of urea is based on the possible redox mechanism with the reduction from Cu^{2+} to Cu^{+}. According to the experimental results, we can provide the basic study for the selective and efficient processing of the CuPc-borophene nanocomposite-based sensor with excellent electrochemical performances. Future research will focus on integrating advanced nanotechnological applications to optimize the design of borophene nanocomposite-based sensors. Also, studies will have a driving force on the design of 2D borophene-based sensors with different morphologies such as switch and multi/demultiplexer. In future work, we strongly believe that borophene-based sensors require investigation to a greater extent with unique properties low-cost and flexibility in biomedical applications.

4 Conclusion

One of the drawbacks of Pcs is their low conductivity. It seems that by a hybrid material formed by a combination of CuPc with a highly conductive material as borophene improved the sensitivity of the sensors. The developed this method can represent an advantageous alternative to other traditional methods for detection of urea. Due to inexpensive, simple, portable, accurate, rapid determination, and the minimum amounts of samples of reagents/solvents, it can be considered an environmentally friendly analytical method. The bands between 1400 and 1600 cm^{-1} in Raman spectrum of borophene can be attributed to inter-icosahedron bonds. The Raman bands of the borophene can be observed in the Raman spectrum of the CuPc: borophene nanocomposite. CuPc-borophene nanocomposite-based non-enzymatic voltammetric electrochemical has higher sensitivity of 10.43 µA/mMcm^2 in voltammetric cycle of 1 min. It may be possible to commercialize the novel CuPc-borophene nanocomposite and CuPc-borophene nanocomposite-based non-enzymatic electrochemical urea sensor. These outputs may enter the global market and provide an opportunity for future fruitful biomedical electronics.

Acknowledgements This study was supported by TUBITAK (Grant Number 120N816).

Declarations

Conflict of interest The authors declare that they have no competing financial and non-financial interest.

References

1. D. Dutta, S. Chandra, A.K. Swain, D. Bahadur, Anal. Chem. **86**, 5914 (2014)
2. A. Sharma, K. Rawat, H.B. Bohidar, P.R. Solanki, Appl. Clay Sci. **146**, 297 (2017)
3. A. Kaushik, P.R. Solanki, A.A. Ansari, G. Sumana, S. Ahmad, B.D. Malhotra, Sens. Actuators, B Chem. **138**, 572 (2009)
4. T.Q.N. Tran, S.W. Yoon, B.J. Park, H.H. Yoon, J. Electroanal. Chem. **818**, 76 (2018)
5. C.C. Buron, M. Quinart, T. Vrlinic, S. Yunus, K. Glinel, A.M. Jonas, B. Lakard, Electrochim. Acta **148**, 53 (2014)
6. K.M. Khan, H. Krishna, S.K. Majumder, P.K. Gupta, Food Anal. Methods **8**, 93 (2014)
7. Z.P. Yang, X. Liu, C.J. Zhang, B.Z. Liu, Biosens. Bioelectron. **74**, 85 (2015)
8. M. Manjula, B. Karthikeyan, D. Sastikumar, Appl. Phys. A **126**, 1 (2020)
9. S. Asgari, N. Granpayeh, T. Fabritius, Opt. Commun. **474**, 126080 (2020)
10. S. Hu, R. Tian, Y. Dong, J. Yang, J. Liu, S. Cao, RSC Adv. **3**, 21447 (2013)
11. M. Shi, Y. Zhao, H. Xu, J. Mack, L. Yin, X. Wang, Z. Shen, RSC Adv. **6**, 71199 (2016)
12. A.M. Master, M. Livingston, N.L. Oleinick, A. Sen Gupta, Mol. Pharm. **9**, 2331 (2012)
13. H. Hayashi, W. Nihashi, T. Umeyama, Y. Matano, S. Seki, Y. Shimizu, H. Imahori, J. Am. Chem. Soc. **133**, 10736 (2011)
14. A. Kumar, J. Brunet, C. Varenne, A. Ndiaye, A. Pauly, Sens. Actuators, B Chem. **230**, 320 (2016)
15. C.B. Yao, Y.D. Zhang, J. Li, D.T. Chen, H.T. Yin, C.Q. Yu, P. Yuan, Opt. Mater. **37**, 80 (2014)
16. C. Salvo-Comino, C. García-Hernández, C. García-Cabezón, M.L. Rodríguez-Méndez, Sensors **18**, 2716 (2018)
17. S. Radhakrishnan, S.D. Deshpande, Sensors **2**, 185 (2002)
18. T. Schwieger, H. Peisert, M.S. Golden, M. Knupfer, J. Fink, Phys. Rev. B **66**, 155207 (2002)
19. M. Ouyang, X. Hu, X. Shao, L. Chen, W. Li, R. Bai, L. Zhang, X. Lv, A. Tameev, C. Zhang, RSC Adv. **9**, 34382 (2019)

20. S.S. Mali, D.S. Dalavi, P.N. Bhosale, C.A. Betty, A.K. Chauhan, P.S. Patil, RSC Adv. **2**, 2100 (2012)
21. M. Della Pirriera, J. Puigdollers, C. Voz, M. Stella, J. Bertomeu, R. Alcubilla, J. Phys. D Appl. Phys. **42**, 145102 (2009)
22. K.I. Ozoemena, T. Nyokong, Electrochim. Acta **51**, 5131 (2006)
23. D. Liu, Y.T. Long, ACS Appl. Mater. Interfaces. **7**, 24063 (2015)
24. Y. Wang, N. Hu, Z. Zhou, D. Xu, Z. Wang, Z. Yang, H. Wei, E.S.W. Kong, Y. Zhang, J. Mater. Chem. **21**, 3779 (2011)
25. B. Wang, X. Zhou, Y. Wu, Z. Chen, C. He, Sens. Actuators, B Chem. **171–172**, 398 (2012)
26. J. Malig, N. Jux, D. Kiessling, J.J. Cid, P. Vázquez, T. Torres, D.M. Guldi, Angew. Chem. Int. Ed. **50**, 3561 (2011)
27. X. Zhou, X. Wang, B. Wang, Z. Chen, C. He, Y. Wu, Sens. Actuators, B Chem. **193**, 340 (2014)
28. Z. Zhang, S.N. Shirodkar, Y. Yang, B.I. Yakobson, Undefined **56**, 15421 (2017)
29. L. Liu, Z. Zhang, X. Liu, X. Xuan, B.I. Yakobson, M.C. Hersam, W. Guo, Undefined **20**, 1315 (2020)
30. Z. Zhang, A.J. Mannix, X. Liu, Z. Hu, N.P. Guisinger, M.C. Hersam, B.I. Yakobson, Sci. Adv. **5**, 9 (2019). https://doi.org/10.1126/sciadv.aax0246
31. Z. Zhang, Y. Yang, E.S. Penev, B.I. Yakobson, Adv. Func. Mater. **27**, 1605059 (2017)
32. Z. Zhang, E.S. Penev, B.I. Yakobson, Chem. Soc. Rev. **46**, 6746 (2017)
33. P. Ranjan, T.K. Sahu, R. Bhushan, S.S.R.K.C. Yamijala, D.J. Late, P. Kumar, A. Vinu, Adv. Mater. **31**, 1900353 (2019)
34. D. Ma, J. Zhao, J. Xie, F. Zhang, R. Wang, L. Wu, W. Liang, D. Li, Y. Ge, J. Li, Y. Zhang, H. Zhang, Nanoscale Horizons **5**, 705 (2020)
35. D. Ma, R. Wang, J. Zhao, Q. Chen, L. Wu, D. Li, L. Su, X. Jiang, Z. Luo, Y. Ge, J. Li, Y. Zhang, H. Zhang, Nanoscale **12**, 5313 (2020)
36. H. Li, L. Jing, W. Liu, J. Lin, R.Y. Tay, S.H. Tsang, E.H.T. Teo, ACS Nano **12**, 1262 (2018)
37. M. Tanhaei, A.R. Mahjoub, V. Safarifard, Ultrason. Sonochem. **41**, 189 (2018)
38. W. Hao, G. Das, H.H. Yoon, J. Electroanal. Chem. **747**, 143 (2015)
39. R. Rahmanian, S.A. Mozaffari, Sens. Actuators, B Chem. **207**, 772 (2015)
40. M. Dervisevic, E. Dervisevic, M. Şenel, Sens. Actuators, B Chem. **254**, 93 (2018)
41. S.G. Ansari, R. Wahab, Z.A. Ansari, Y.S. Kim, G. Khang, A. Al-Hajry, H.S. Shin, Sens. Actuators, B Chem. **137**, 566 (2009)
42. S. Selvarajan, A. Suganthi, M. Rajarajan, Ultrason. Sonochem. **42**, 183 (2018)
43. I. Gürol, M. Durmuş, V. Ahsen, Eur. J. Inorg. Chem. **2010**, 1220 (2010)
44. C. Taşaltın, T.A. Türkmen, N. Taşaltın, S. Karakuş, J. Mater. Sci. Mater. Electron. **32**(8), 10750 (2021)
45. Z. Li, T. Zhuang, J. Dong, L. Wang, J. Xia, H. Wang, X. Cui, Z. Wang, Ultrason. Sonochem. **71**, 105384 (2021)
46. F. Peng, S.J. Qin, L.F. Hu, J.Y. Wang, J.M. Yang, X.Q. Chen, G.B. Pan, Chem. Phys. Lett. **652**, 6 (2016)
47. S.K. Das, A. Bedar, A. Kannan, K. Jasuja, Sci. Rep. **5**, 10522 (2015). https://doi.org/10.1038/srep10522
48. T.H. Le, Y. Oh, H. Kim, H. Yoon, Chem. Eur. J. **26**, 6360 (2020)
49. G. Sachdeva, S. Kaur, R. Pandey, S.P. Karna, Computation **9**(9), 101 (2021)
50. S. Mustapha, M.M. Ndamitso, A.S. Abdulkareem, J.O. Tijani, D.T. Shuaib, A.K. Mohammed, A. Sumaila, Adv Nat Sci Nanosci Nanotechnol **10**, 045013 (2019)
51. A.L. James, K. Jasuja, RSC Adv. **7**, 1905 (2017)
52. S.K. Das, A. Bedar, A. Kannan, K. Jasuja, Sci. Rep. (2015). https://doi.org/10.1038/srep10522
53. G.R. Monama, K.D. Modibane, K.E. Ramohlola, K.M. Molapo, M.J. Hato, M.D. Makhafola, G. Mashao, S.B. Mdluli, E.I. Iwuoha, Int. J. Hydrogen Energy **44**, 18891 (2019)
54. M. Samanta, M. Mukherjee, U.K. Ghorai, C. Bose, K.K. Chattopadhyay, Mater. Res. Bull. **123**, 110725 (2020)
55. B.B. Topuz, G. Gündüz, B. Mavis, Ü. Çolak, Dyes Pigm. **96**, 31 (2013)
56. F. Sánchez-De La Torre, J. Rivera De La Rosa, B.I. Kharisov, C.J. Lucio-Ortiz, Materials **6**, 4324–4344 (2013)
57. G. Parakhonskiy, N. Dubrovinskaia, L. Dubrovinsky, S. Mondal, S. van Smaalen, J. Cryst. Growth **321**, 162 (2011)
58. J. Qin, T. Irifune, H. Dekura, H. Ohfuji, N. Nishiyama, L. Lei, T. Shinmei, Phys. Rev. B Condens. Matter Mater. Phys. **85**, 014107 (2012)
59. Z.X. Sun, Y.Y. Wu, X.X. Han, G.J. Zhang, X.F. Liu, CrystEngComm **19**, 3947 (2017)
60. C.K. Choi, S.M. Shaban, B.S. Moon, D.G. Pyun, D.H. Kim, Anal. Chim. Acta **1170**, 338630 (2021)
61. B. Öndeş, F. Akpınar, M. Uygun, M. Muti, D. Aktaş Uygun, Microchem. J. **160**, 105667 (2021)
62. R.K. Sajwan, P. Sharma, G.B.V.S. Lakshmi, P.R. Solanki, Mater. Lett. **305**, 130794 (2021)
63. E. Muthusankar, V.K. Ponnusamy, D. Ragupathy, Synth. Met. **254**, 134 (2019)
64. R.-an Doong, H.-m Shih, Biosens. Bioelectron. **25**, 1439 (2010)
65. O. Akhavan, E. Ghaderi, J. Mater. Chem. **21**, 12935 (2011)